# EFFECT OF THE SOLVENT ON THE CONFORMATIONAL PROFILE OF BALARAM's PEPTIDE: A COMPUTATIONAL STUDY

**Patricia Gomez-Gutierrez[1], Jaime Rubio-Martinez[2] and Juan J. Perez[1,*]**

[1]Dept. of Chemical Engineering. ETSEIB. Universitat Politecnica de Catalunya-Barcelona Tech, Barcelona, Spain

[2]Department of Materials Science and Physical Chemistry, University of Barcelona and the Institut de Recerca en Quimica Teorica i Computacional (IQTCUB), Barcelona, Spain

***Corresponding author: juan.jesus.perez@upc.edu**

Av. Diagonal, 647. 08028 Barcelona, Spain

**keywords: solvent effects; conformational profile; Balaram's peptide; computer simulations;**

**ABSTRACT**

The present work reports the results of a computational study aimed at characterizing the conformational profile of the Balaram's peptide (Ace-Leu-Val-Val-Aib-Gly-Leu-Val-Val-NHMe) in different solvents, including chloroform, dimethyl sulfoxide, methanol and water. For this purpose, 10 μs molecular dynamics trajectories were computed in explicit solvent for each system, starting from an extended conformation. The results of the present study confirm previous NMR and CD findings, providing the excuse to fine-tune the conclusions achieved then. Present results show that the peptide exhibits a helical conformation in chloroform, but a mixture of β-hairpin and Ω-shape conformations, as the predominant structures in DMSO and MeOH. Finally, the peptide does not exhibit a preferred conformation in water, although significant populations of helical and β-hairpin conformations are available. Present results underline the role of the solvent on the conformational profile of a peptide and it is an example of the complementarity between computational methods and spectroscopy studies.

## INTRODUCTION

Peptides are important mediators in cell-to-cell communication, eliciting actions as hormones, neurotransmitters or immunomodulators and consequently, involved in the regulation of many physiological processes [1]. They can also act as modulators of protein-protein interactions, acting as surrogates of protein epitopes [2,3]. The wide range of activities performed is the result of their stereochemical features that makes them suitable for selectively binding diverse receptors, enabling them to afford an ample diversity of functions. Accordingly, a profound understanding of their structural features is pivotal to explain their biological activity and important for opening new frontiers in peptide science [4,5] through the design of new surrogates and peptidomimetics to render new applications [6,7].

In contrast to most proteins, short peptides do not usually exhibit a native structure in solution due to their flexible nature. However, their conformational profile cannot be simply described as a random coil, since peptides exhibit local structural features [8-11]. Actually, the conformational profile of a peptide is better described as an ensemble of structures, populated according to their relative free energy and the temperature of the system. Accordingly, spectroscopy studies on the conformational features of peptides are limited to provide ensemble-averages of different conformations that can be unraveled with the use of complementary computational methods. Moreover, peptides may exhibit different conformational profile in diverse environments, concluding that the environment induces changes in the ensemble of conformations. There are examples in the literature reporting peptides adopting different conformations in diverse solvents [12, 13], adopt receptor bound conformations different to those exhibited in solution [14, 15] or intrinsically disorder protein epitopes that acquire a specific conformation when bound [16, 17].

The ensemble conformational profile exhibited by a peptide is determined by the set of low energy conformations attainable at a specific temperature. Moreover, solvents may alter the accessibility to diverse low energy conformations, in such a way that it can even lead to the disappearance and/or emergence of specific ones. This is clearly illustrated by the changes observed on the conformational profile of the alanine

dipeptide [18,19]. Specifically, comparison of the Ramachandran maps of the alanine dipeptide in diverse solvents shows that in chloroform the profile is similar to the one observed *in vacuo*, whereas in solvents with higher dielectric constant and diverse capacity to establish intermolecular hydrogen bonds, like water or methanol the profile changes dramatically. This differential behavior is attributable to the characteristics of the solvent [19] and their effect on the balance of intramolecular and intermolecular interactions between the peptide and the solvent [18]. The former are linked to the intrinsic conformational features of the peptide and are dictated by its amino acid sequence, whereas solvent features determine intermolecular interactions modulating the peptide conformational profile.

About twenty years ago, P. Balaram et al. [12] reported the results of an experimental study aimed at understanding the conformational features of the peptide Boc-Leu-Val-Val-Aib-Gly-Leu-Val-Val-OMe (Boc: t-butyloxycarbonyl; Aib= $\alpha$-aminoisobutyric acid; OMe: methyl ester), designed to adopt different conformations in diverse solvents. The design rationale lies on the observation that the dipeptide Aib-Gly induces the peptide backbone to attain β-turn conformations that could act as a nucleus capable to induce the peptide to adopt different conformational states including hairpins and helical structures. Furthermore, since residues with polar side chains are excluded from the design, the peptide offers the opportunity to focus on the ability of the backbone to establish intermolecular interactions with the solvent, defining the conformational profile of the peptide chain. After NMR and CD spectroscopy studies, the authors concluded that the peptide predominantly adopts a helical conformation in chloroform, whereas in solvents like methanol (MeOH) or dimethylsulfoxide (DMSO) it exhibits an appreciable population of β-hairpin conformations [12].

Following the discussion outlined in the previous paragraphs, we considered interesting to unravel the role played by the solvent on inducing changes on the peptide ensemble of conformations through computational studies [20-22]. Therefore, the present work describes the results of a series of molecular dynamics simulations of the octapeptide (Balaram's peptide) in diverse explicit solvents including chloroform, DMSO, MeOH and water to discuss the role played by the solvent, determined by their

specific features. Specifically, the conformational profile of the Balaram's peptide in diverse solvents was assessed by means of 10μs molecular dynamics (MD) simulations at 300K. Simulations were carried out on a model peptide consisting of the octapeptide capped with an acetyl group at the N-terminus and a methylamide at the C-terminus, as shown in Figure 1.

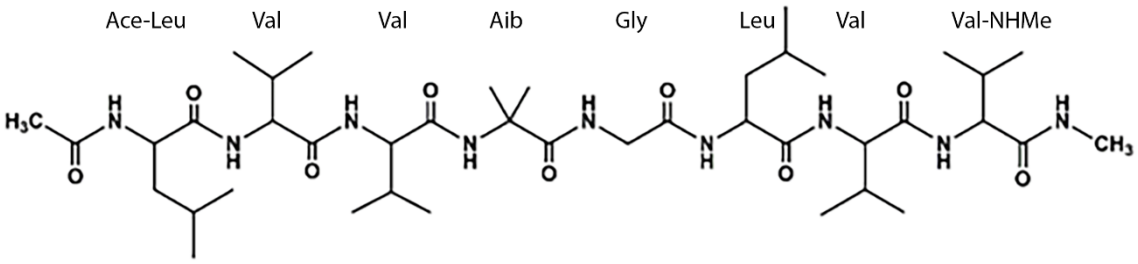


**Figure 1.** Chemical structure of the model peptide object of the present study with sequence: Ac-Leu-Val-Val-Aib-Gly-Leu-Val-Val-NHMe.

## METHODS

The peptide, in its extended conformation was soaked in parallelepiped boxes of different size (Table S1) containing equilibrated chloroform [23], DMSO [24], MeOH [25] and water [26], respectively. Calculations were carried out with the AMBER16 suit of programs [27], using the ff12SB force field [28] in a NVT collective and using periodic boundary conditions. The systems were energy minimized through 3000 steps of the steepest descent method, followed by the conjugate gradient method to remove possible steric clashes. After minimization, the systems were heated to 300K using MD in the NVT collective at a rate of 30K per 10ps. Subsequently, the systems were equilibrated for 1 ns within the NPT collective using the Berendsen's barostat [29], followed by 10 μs production run within the NVT collective, keeping the temperature at 300K by means of the Langevin thermostat with a collision frequency of 2 $ps^{-1}$. A cutoff of 10Å to treat non-covalent interactions, whereas electrostatic interactions were treated using the PME method [30]. The SHAKE algorithm was used in all the MD simulations to constrain bonds involving hydrogen atoms that permitted to use an integration step of 2fs [31].

Principal Component Analysis (PCA) [32] was used to analyze the results of the MD calculations. Accordingly, for each simulation all the snapshots were superimposed to the first one produced after equilibration, using the coordinates of the C$\alpha$ of the

diverse residues to compute a covariance matrix. To rationalize the conformational profile of the Balaram's peptide, the free-energy landscape projected onto the principal components PC1 and PC2 was computed. In this representation, free energy differences are given by the equation 1:

$$\Delta G = -k_b T \ln(P_i/P_{max}) \qquad \text{Equation 1}$$

where $(P_i/P_{max})$ refers to the number of configurations located in bin *i*, relative to the number contained in the most populated bin. In addition, in order to identify the set of conformations attained by the peptide, we carried out a hierarchical cluster analysis of the structures using of the average link algorithm [33]. For this purpose, the root-mean-square deviation of the peptide backbone using the C$\alpha$ of the diverse residues was used as a measure of the distance between two conformations.

The time-dependent secondary structure per residue along the MD trajectory was computed by means of the DSSP procedure [34] using the cpptraj program embedded in AMBER16 [27]. Analysis of the plots provides a quick look of the conformational exchange produced during the sampling process.

Solvent radial distribution functions were also computed using the cpptraj program embedded in the AMBER16 suit of programs [27]. The area under the peaks yields the number of solvent molecules surrounding a specific atom in the solvation shell, averaged over the sampling process. Moreover, taking into account the hydrophobic nature of the peptide side chains of the Balaram's peptide, the area under the peak provides insight into the involvement of peptide backbone atoms in intermolecular interactions with solvent molecules.

## RESULTS

### *Simulation in chloroform*

Analysis of peptide conformational profile was carried out using 1,000,000 structures extracted from the 10μs molecular dynamics simulation, taken at regular time intervals. The set of Cartesian coordinates from the C$\alpha$ atoms of the central peptide segment, including residues from $Val^2$ to $Val^7$, permitted to align the structures collected during the sampling process. Superposition of the structures was used to compute atom

fluctuations and subsequently, a covariance matrix that was diagonalized to obtain its principal components [32]. Figure 2 shows pictorially the free energy landscape projected onto the two first principal components (PC1 and PC2). Inspection of Figure 2 shows 3 basins on the low dimensional representation of the free energy landscape.

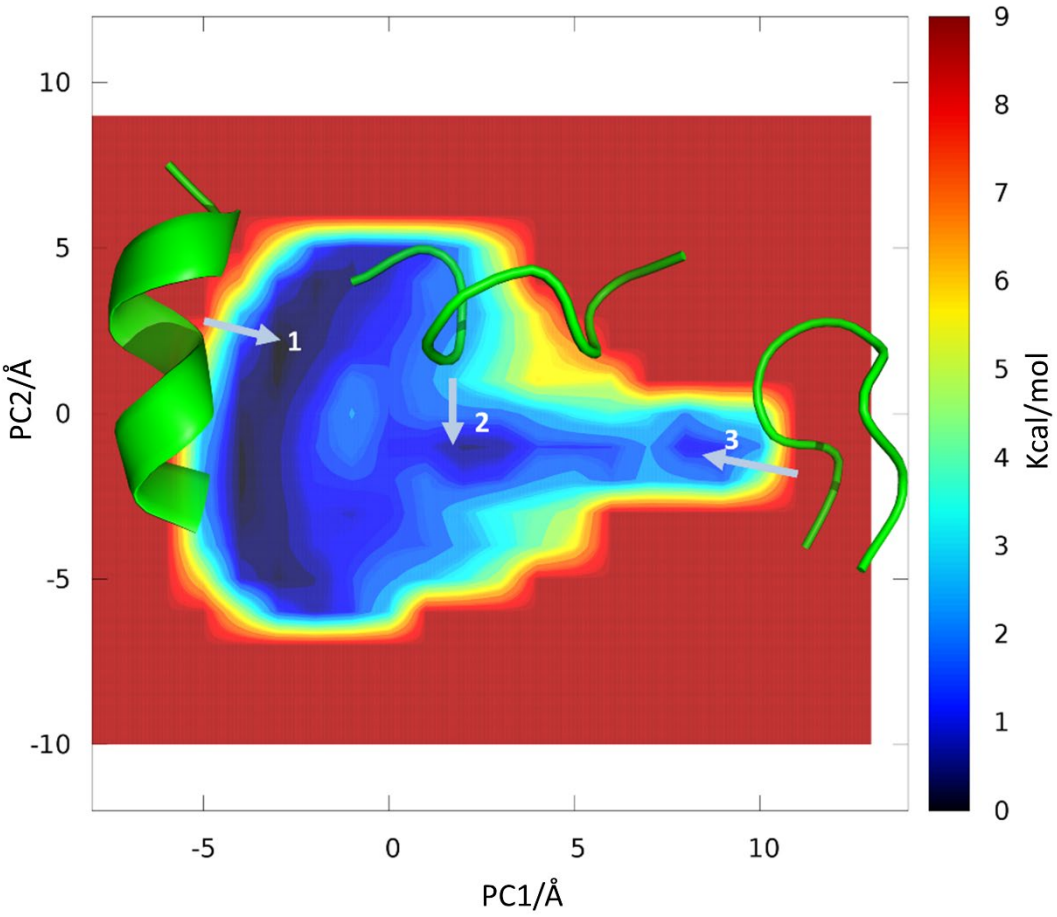


**Figure 2.** Projection of the peptide configurations sampled during the MD calculation in chloroform onto the space defined by the two first Principal Components. Relative free energies are depicted in a color code being dark blue the lowest, in such a way that three low energy basins can be distinguished. Arrows indicate the position of the lowest energy point in each of the basins, together with the associated structure depicted in a ribbon representation.

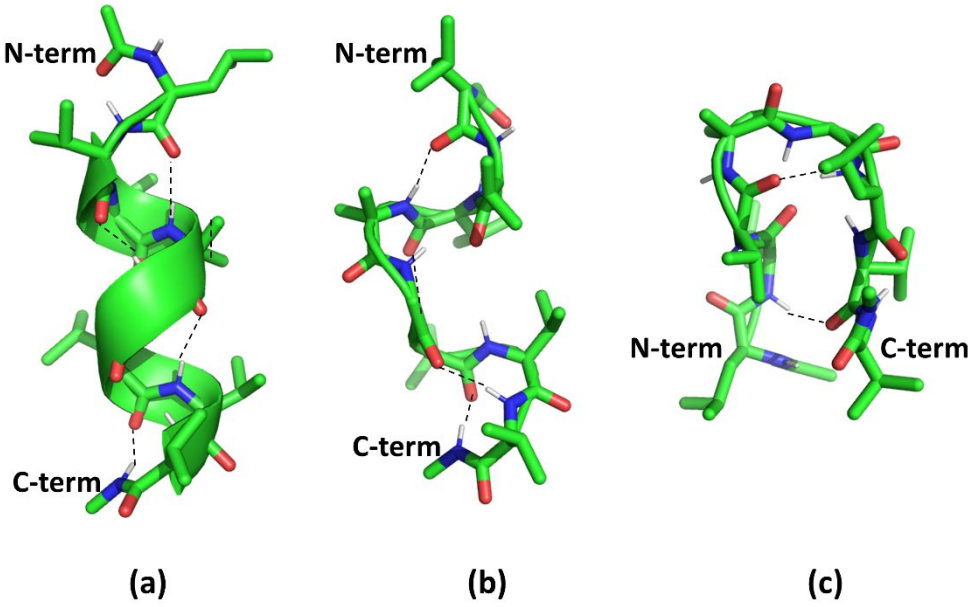


**Figure 3.** Structures of lowest energy conformations identified in the chloroform sampling, where dotted lines represent hydrogen bonds, using as default geometrical features a distance (O…H) ∈[2.0-3.0Å] and a NH…O angle <180°. a) minimum#1 is a $3_{10}$ helical structure with a pattern of hydrogen bonds between carbonyl oxygen of residue i and amide hydrogen of residue i+3; b) minimum#2 is an intermediate structure showing diverse β-turns with their associated hydrogen bonds; c) minimum#3 is a hairpin structure including a β-turn involving residues (3-6), reinforced by a hydrogen bond between the amide hydrogen of $Val^2$ and the carbonyl oxygen of $Val^7$.

The lowest energy minimum is located at coordinates (-3,2) in a large low energy basin that covers ~80% of peptide population, according to the cluster analysis. Structures in this basin are helical, showing a backbone hydrogen bond pattern between the carbonyl oxygen of residue i and the amide hydrogen in residue i+3, consistent with a $3_{10}$ helix, as can be seen in Figure 3a. The following low energy basin has its lowest energy point located at coordinates (2,-1) and accounts for ~16% of peptide population, as deduced from the cluster analysis. Structures in this basin adopt Ω-shape conformations. More specifically, these structures typically exhibit a central β-turn reinforced by a hydrogen bond between the carbonyl oxygen of $Val^3$ and the hydrogen amide of $Leu^6$ that is flanked by two β-turns at both termini, as shown in Figure 3b. Finally, the following low energy basin has its lowest energy point located at coordinates (8,-1) and accounts for ~3% of the population, as deduced from the cluster analysis. The representative structure is a hairpin turn consisting of a β-turn involving the segment

Val[3]-Leu[6] with a hydrogen bonds between the carbonyl oxygen of Val[3] and the amide hydrogen of Leu[6] and the amide hydrogen of Val[2] and the carbonyl oxygen of Val[7] (Figure 3c).

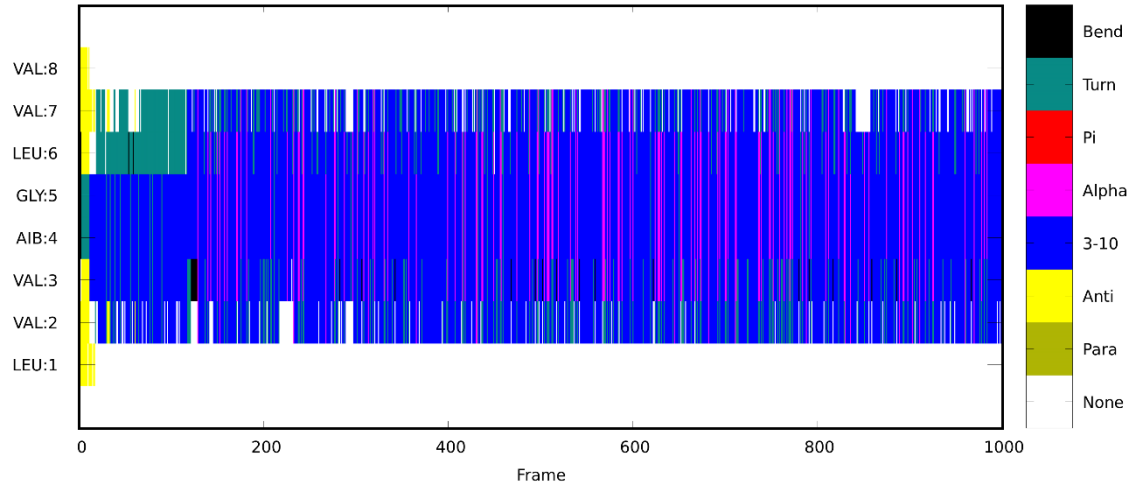


**Figure 4.** Time-dependent evolution of the secondary structure in chloroform computed taking one snapshot every 10 ns at regular intervals. Calculations were performed using the DSSP procedure [34].

Figure 4 shows the time-dependent evolution of the secondary structure per residue during the sampling process, computed using the DSSP procedure [34]. A can be seen, the peptide adopts a hairpin conformation after energy minimization that is preserved for around 200 ns. During the following μs the peptide adopts an intermediate structure and subsequently, the peptide adopts a $3_{10}$ helix that is kept during the rest of the simulation. Interestingly, although the $3_{10}$ helix is the most frequent helical structure sampled, $\alpha$-helices are also observed during the sampling process. Inspection of Figure 4 suggests that the peptide goes through conformational changes anticipated by the free energy surface, with population estimates of the diverse conformations that agree well with the results of the cluster analysis. However, the diverse conformations are sampled in a sequential manner, in such a way that it can be said that when the simulation runs long enough the peptide adopts basically helical structures in this solvent.

Solvent radial distribution functions around residues of the central peptide segment provide further insight into the involvement of the diverse peptide bonds in inter- or intra-molecular interactions. Figures 5 and 6 depict radial distributions of chloroform molecules around peptide bonds in the peptide central segment, including residues 2 to 7.

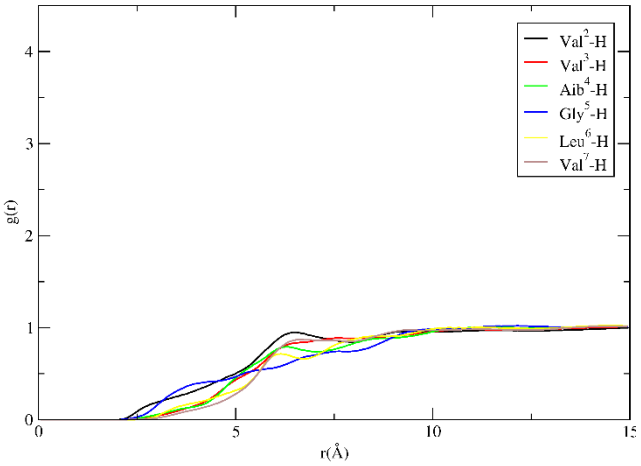


**Figure 5.** Radial distributions of chloroform molecules (Cl atoms) around diverse backbone amide hydrogens of the peptide central segment including residues 2-7.

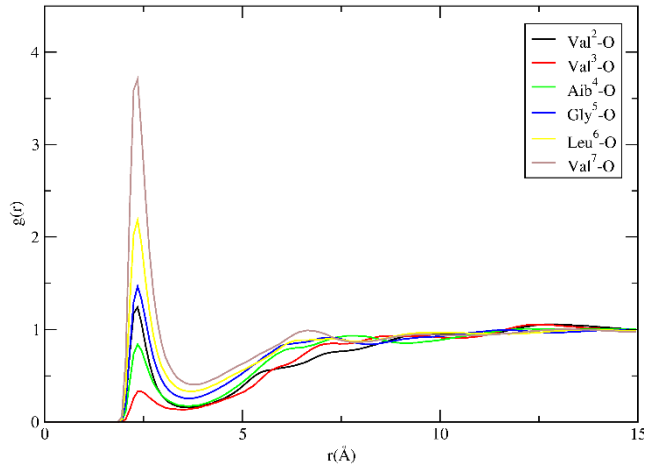


**Figure 6.** Radial distributions of chloroform molecules (H atom) around diverse backbone amide oxygens of the peptide central segment including residues 2-7.

Inspection of Figure 5 shows a limited solvent structure around the different residues, underlying that amide hydrogens are not involved in intermolecular interactions with the solvent. On the other hand, inspection of Figure 6 shows solvent peaks around carbonyl oxygens at 2.5 Å. Specifically, Val[3] and Aib[4] oxygens are the least exposed according to their smaller integration area. Moreover, the Val[7] oxygen is the most exposed, consistent with the fact that it does not take part of the helical structure for about half of the sampling time and Leu[6] oxygen shows also higher exposure due to the open structure attained by the peptide during the first μs. These results support that peptide bonds of the central segment are mostly involved in intramolecular interactions during the sampling process, consistent with a predominant helical structure of the peptide chain in this solvent.

Complementary, Figure 7a shows the time evolution of the distance between the Val[3] carbonyl oxygen and the Leu[6] hydrogen amide, whereas Figure 7b shows the time evolution of the distance between Aib[4] carbonyl oxygen and the Val[7] amide hydrogen. Figure 7a shows a distance consistent with a hydrogen bond during the whole sampling process, whereas Figure 7b shows a distance consistent with a hydrogen bond only after the first μs. Accordingly, except for the first μs, the rest of the time the peptide exhibits two consecutive β-turns and taking into account the conformations attained in the sampling period (Figure 3), this result provides further support for the peptide attaining a helical conformation. Moreover, the first μs sampling time can be interpreted as if the peptide is blocked in a kinetic trap before it reaches a helical conformation.

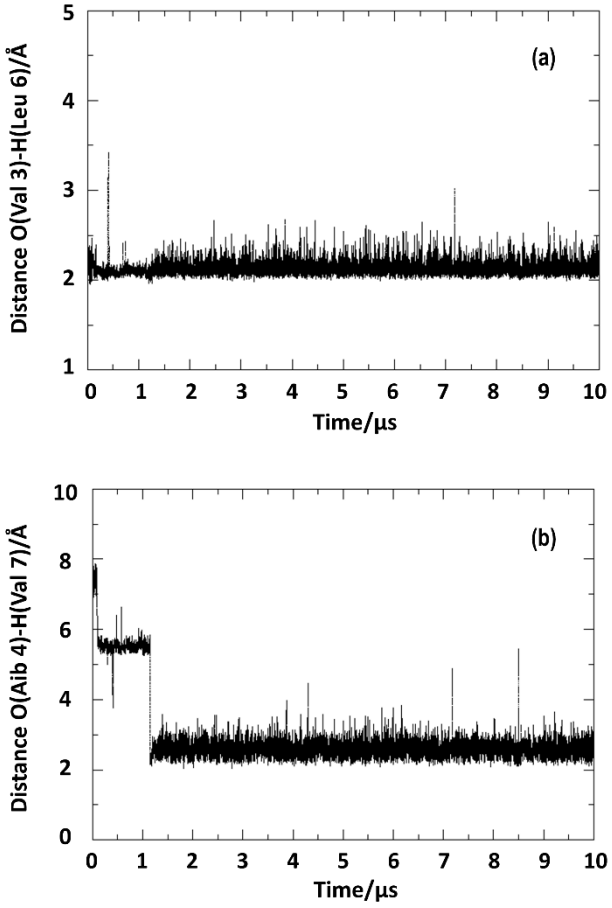


**Figure 7.** Atomic distance time evolution for the simulation in chloroform. a) between Val[3] carbonyl oxygen and Leu[6] amide hydrogen; b) between Aib[4] carbonyl oxygen and Val[7] amide hydrogen.

*Simulation of the peptide in DMSO*

The same procedure as explained above was used to analyze the MD trajectory of the peptide in DMSO. Figure 8 shows pictorially the projection of the 1,000,000 snapshots onto the subspace defined by the two first principal components (PC1 and PC2). Inspection of Figure 8 shows four basins on the low dimensional representation of the free energy landscape.

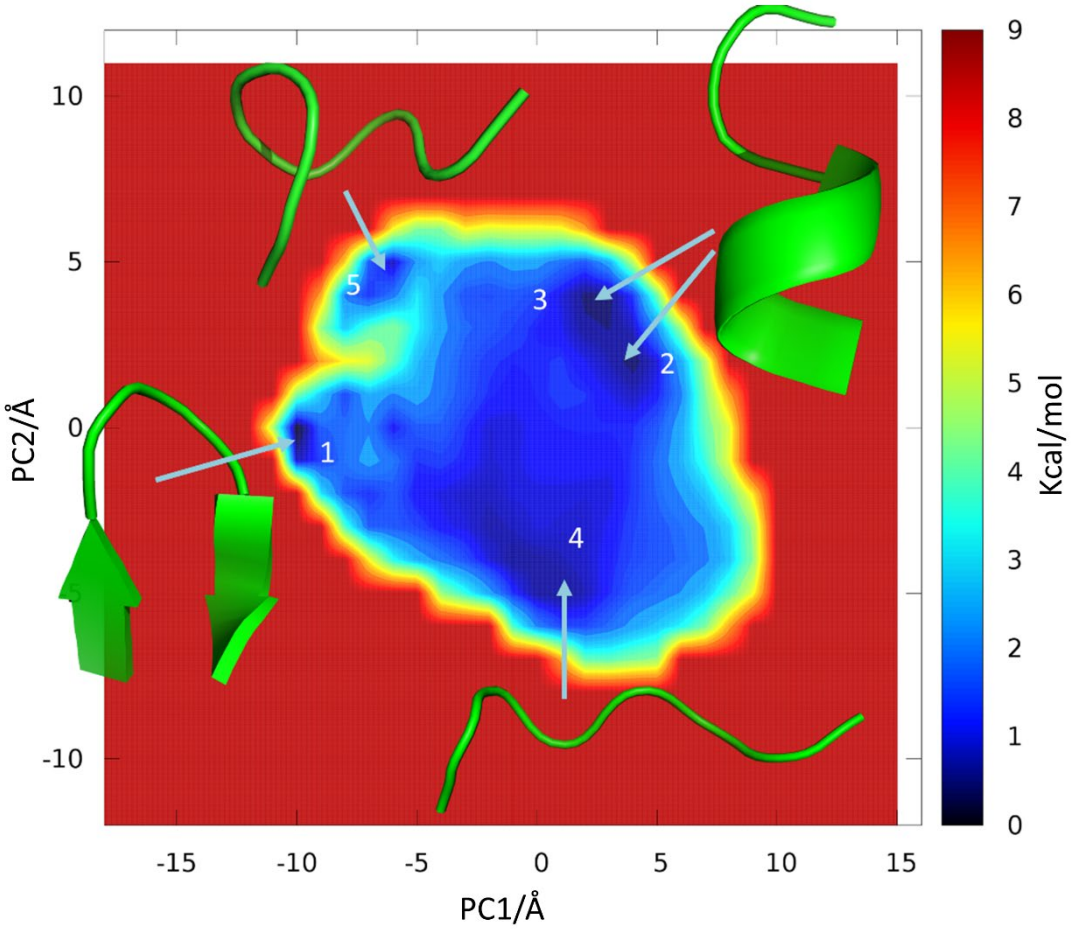


**Figure 8.** Projection of the peptide configurations sampled during the MD calculation in DMSO onto the space defined by the two first Principal Components. Relative free energies are depicted in a color code being dark blue the lowest, in such a way that four low energy basins can be distinguished. Arrows indicate the position of the lowest energy point in each of the basins, together with the associated structure depicted in a ribbon representation.

The lowest energy basin exhibits its minimum located at coordinates (-10,0) and accounts for a ~21% of the population, as deduced from the cluster analysis. Structures in this basin correspond to well-defined hairpin turns exhibiting hydrogen bonds between the carbonyl oxygen of $Leu^{1}$ and the amide hydrogen of $Val^{8}$, the amide hydrogen of $Val^{3}$ and the carbonyl oxygen of $Leu^{6}$ and the carbonyl oxygen of $Val^{3}$ and the amide hydrogen of $Leu^{6}$, as shown pictorially in Figure 9a. Low energy minima #2 and #3 are located at coordinates (4,2) and (3,4), respectively are part of the same basin that accounts for ~27% of the population as deduced from the cluster analysis. Structures in this basin are helical at the C-terminus as shown in Figure 9b, exhibiting a pattern of

hydrogen bonds between the carbonyl oxygen of residue i and the amide hydrogen in residue i+4. Low energy minimum #4 is located in a vast basin at coordinates (1,-5), accounting for a population of ~47%, as deduced from the cluster analysis. Structures in this basin exhibit a Ω-shape conformation with a β-turn in its central segment, reinforced by a hydrogen bond between the carbonyl oxygen of $Val^3$ and the amide hydrogen of $Leu^6$ and flanked by γ-turns or PPII conformations at both termini, as shown pictorially in Figure 9c. Finally, low energy minimum #5 is located at coordinates (-6, 5) in a shallow basin that accounts for ~5% of the population, as deduced from the cluster analysis. Structures in this basin represent intermediate structures between helix and β-hairpin turn, adopting shapes that remind the runner of a sled, as shown in Figure 9d.

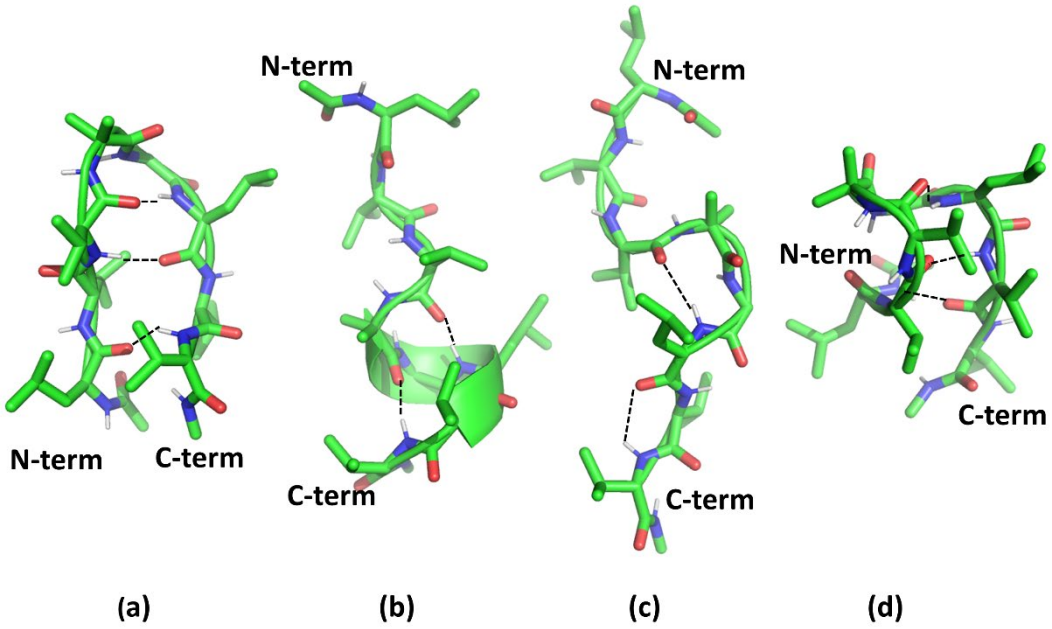


**Figure 9.** Structures of lowest energy conformations identified in the DMSO sampling, where dotted lines represent hydrogen bonds using as default geometrical features a O…H distance [2.0-3.0Å] and a NH…O angle <180°. a) minimum#1 is a hairpin structure exhibiting hydrogen bonds $Leu^1$(C=O)…(NH)$Val^8$; $Val^3$(NH)…(C=O)$Leu^6$; and $Val^3$(C=O)…(NH)$Leu^6$; b) minima #2 and #3 is a helical structure at the C-terminus exhibiting a pattern of hydrogen bonds between the carbonyl oxygen of residue i and the amide hydrogen in residue i+4; c) minimum 4 corresponds to a Ω-shape conformation with a central β-turn reinforced by a hydrogen bond $Val^3$(C=O)…(NH)$Leu^6$, flanked by PPII or ϒ-turns at the termini; d) minimum#5 can be considered as an intermediate structure.

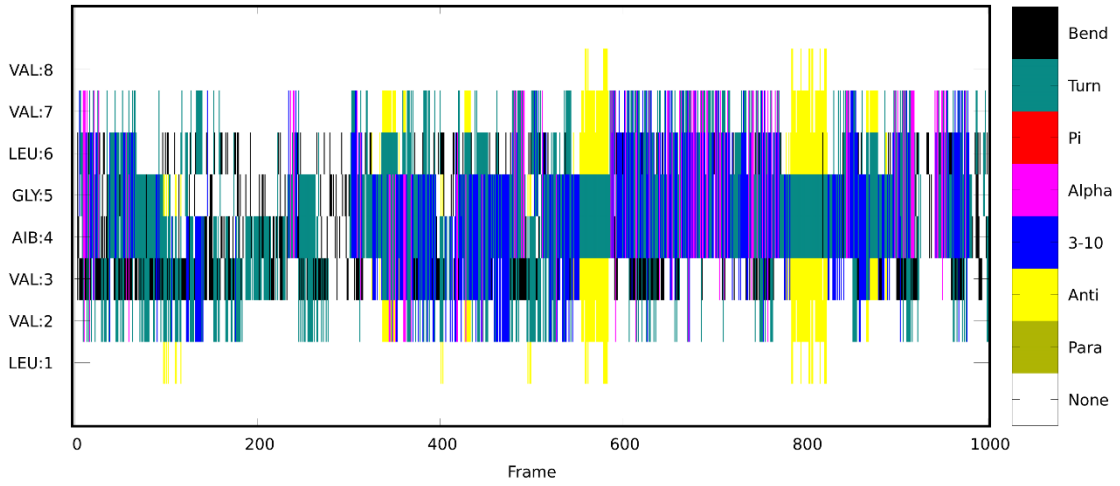


**Figure 10.** Time-dependent evolution of the secondary structure in DMSO computed taking one snapshot every 10 ns at regular intervals. Calculations were performed using the DSSP procedure [34].

Figure 10 shows the time-dependent evolution of the secondary structure per residue during the sampling process, computed using the DSSP procedure [34]. As can be seen, the peptide adopts a hairpin structure at different points of the trajectory including frames 100, 340, 400, 500, 550, 800 and 850 covering a total of ~20% of the sampling. The peptide also adopts helical structures at different points of the MD trajectory. Interestingly, the peptide frequently adopts $3_{10}$ or $\alpha$-helical structures located at the central and C-terminal residues, clearly visible between frames 600-800, covering ~20% of the sampling process. In addition, the peptide also adopts $3_{10}$ structures located at the N-terminus and central segment residues, clearly visible between frames 300-500. In addition to these structures, many conformations can be classified as Ω-shaped, being identified by a bend at $Val^3$ followed by a turn or not at $Aib^4$ covering a big segment of the sampling process, whereas the rest can be considered as intermediate structures.

Analysis of the solvent radial distributions provides further insight into the conformational profile of the peptide. Figure 11 depicts the radial distributions of DMSO molecules around the peptide central segment residues. These functions were computed using the positions of the hydrogen amides of diverse residues of the peptide central segment, including residues 2 to 7, and the oxygen atom of DMSO. Distributions show a similar shape with a sharp peak around 2 Å. Peaks have intensities between 1.6 and 4.1, suggesting that amide hydrogens of residues Val$^{2}$-Val$^{3}$-Aib$^{4}$-Gly$^{5}$ and Val$^{7}$ are highly solvent exposed and, consequently, involved in intermolecular interactions with the solvent during the simulation. The lowest peak is shown around Leu$^{6}$, suggesting that its carbonyl oxygen is more frequently involved in intramolecular interactions during the sampling time. This is consistent with the peptide adopting a β-turn conformation, stabilized by a hydrogen bond between the amide hydrogen of Leu$^{6}$ and the carbonyl oxygen of Val$^{3}$. Moreover, the helical conformation

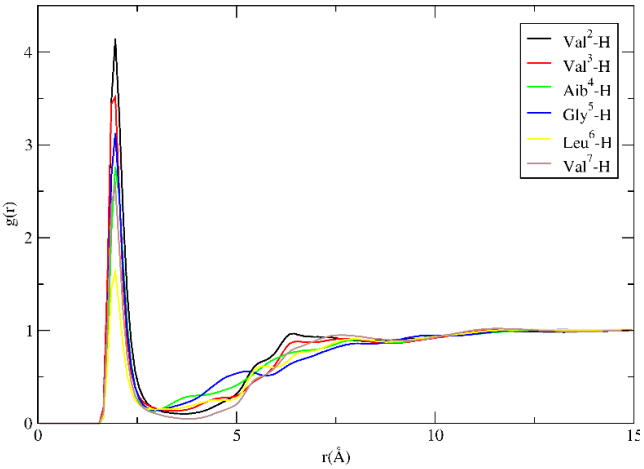


**Figure 11.** Radial distributions of DMSO molecules (O atom) around diverse backbone amide hydrogens of the peptide central segment, including residues 2-7.

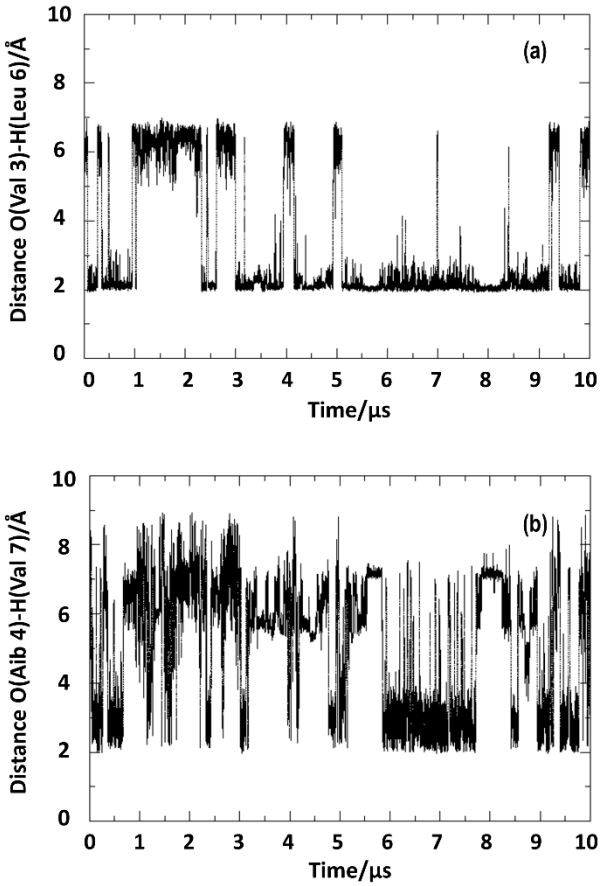


**Figure 12.** Atomic distance time evolution for the simulation in DMSO. a) between Val$^{3}$ carbonyl oxygen and Leu$^{6}$ amide hydrogen; b) between Aib$^{4}$ carbonyl oxygen and Val$^{7}$ amide hydrogen.

can be discarded as the most populated, since it would require that additional hydrogen amides were not exposed to the solvent, which not the case. However, the helical conformation is moderately sampled, since $Val^7$ radial distribution exhibits a smaller area than the rest, supporting that the amide hydrogen may be transiently involved in intramolecular interactions compatible with a helical conformation at the C-terminus.

We also analyzed the time evolution of the distance between the $Val^3$ carbonyl oxygen and the $Leu^6$ hydrogen amide (Figure 12a), as well as the distance between $Aib^4$ carbonyl oxygen and $Val^7$ amide hydrogen (Figure 12b). As can be seen, the distance in the former is consistent with a hydrogen bond ~80% of the sampling time, whereas in the latter exhibits lesser occupancy. Inspection of Figure 12b shows that roughly speaking distances adopted correspond to two values, either ~3 Å or 6-7 Å. Moreover, looking at a specific snapshot we can make an analysis of the distances simultaneously adopted and understand the conformational changes the peptide undergoes. Thus, there are intervals where the two distances simultaneously adopt values of ~3 Å, mainly in the interval 3.7 - 4.6 μs and 6 – 7.5 μs that are consistent with a helical structure as corroborated by inspection of Figure 10. However, there are intervals when the former takes values 3-4 Å and the latter 6-7 Å that correspond more likely to hairpin turns. We can identify these structures in the intervals between the 3.5 μs and the 5.8 μs, and later, in the interval 7.8 - 8.5 μs as corroborated by inspection of Figure 10. Finally, when the former distance is 6-7 Å and the latter is 3-4 Å the structure corresponds to a local β–turn at the C-terminus and, when both are 6-7 Å the structure should be considered as extended.

*Simulation in methanol*

The same methodology as described above was used to analyze the sampling of the peptide in methanol. Figure 13 shows pictorially the projection of the 1,000,000 snapshots onto the subspace defined by the two first principal components (PC1 and PC2). Inspection of Figure 13 permits to identify 5 basins on the low dimensional representation of the free energy landscape. The representative structures of the configurations of each basin are also depicted in a ribbon representation.

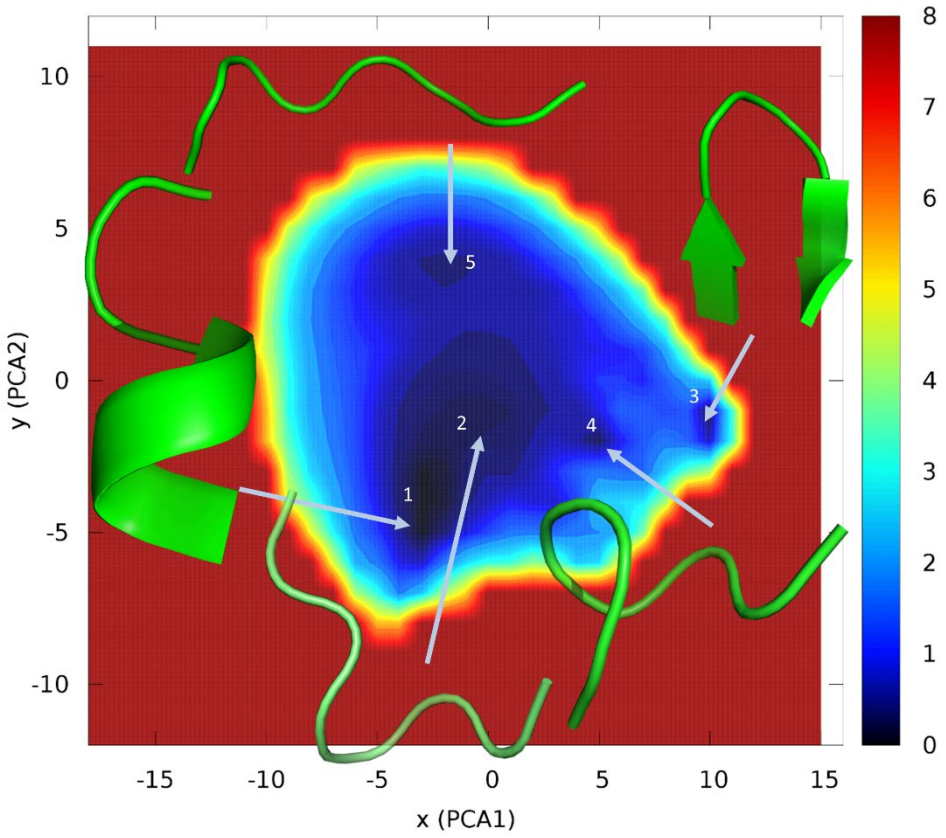


**Figure 13.** Projection of the peptide configurations sampled during the MD calculation in MeOH onto the space defined by the two first Principal Components. Relative free energies are depicted in a color code being dark blue the lowest, in such a way that five low energy basins can be distinguished. Arrows indicate the position of the lowest energy point in each of the basins, together with the associated structure depicted in a ribbon representation.

Minimum #1, located at coordinates (-3,-5) is the lowest energy point in an narrow energy basin that accounts for a ~14% of the population. The basin contains helical structures at the C-terminus that exhibit a pattern of hydrogen bonds between the carbonyl oxygen of residue i and the amide hydrogen in residue i+4, as shown in Figure 14a. Minimum #2 is located at coordinates (-1,-1) in a large basin that accounts for ~62% of the population, as deduced from the cluster analysis. Structures in this basin adopt a Ω shape structure with a central β-turn reinforced by a hydrogen bond between the carbonyl oxygen of $Val^3$ and the amide hydrogen of $Leu^6$, with two additional β-turns at both termini (Figure 14b). Minimum #3, is the lowest energy minimum is located at coordinates (10,-1), in a basin that accounts for ~9.5% of the structures, as deduced from the cluster analysis. Structures in this basin correspond to well defined hairpin turns, exhibiting hydrogen bonds between the carbonyl oxygen of $Leu^1$ and the amide

hydrogen of Val[8], the amide hydrogen of Val[3] and the carbonyl oxygen of Leu[6] and the carbonyl oxygen of Val[3] and the amide hydrogen of Leu[6], as shown in Figure 14c. Minimum #4 is located at coordinates (5,-2) in a shallow basin that covers ~11.5% of the population, according to the cluster analysis. Structures in this basin correspond to intermediate between helix and β-hairpin (Figure 14d). Finally, minimum#5 is located at coordinates (-2,4) in a basin that accounts for ~4% of the conformations, as deduced from the cluster analysis. Structures in this basin are more extended (Figure 14e).

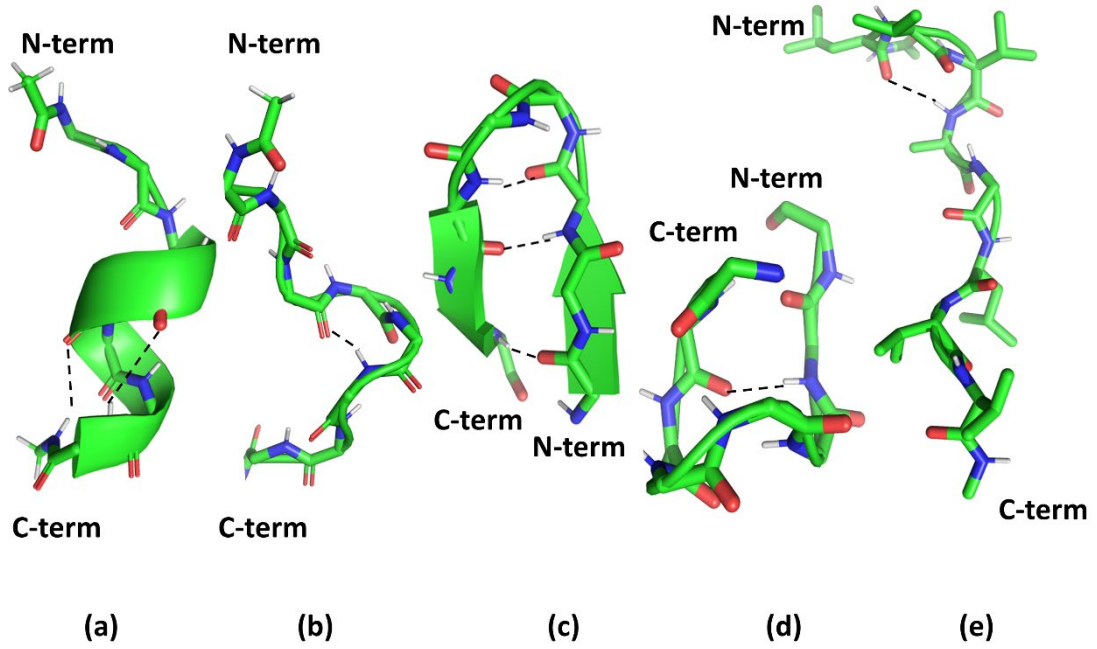


**Figure 14.** Structures of lowest energy conformations identified in the MeOH sampling where dotted lines represent hydrogen bonds using as default geometrical features a O…H distance [2.0-3.0Å] and a NH…O angle <180°. a) minimum#1 (Figure 13), is a helical structure at the C-terminus, exhibiting a pattern of hydrogen bonds between the carbonyl oxygen of residue i and the amide hydrogen in residue i+4. b) Ω-shape conformation with a central β-turn reinforced by a hydrogen bond Val[3](C=O)…(NH)Leu[6], exhibited by most of the structures in the basin containing minimum#1 and covering ~69% of the population; c) minima #2 is a hairpin structure; d) minimum#3 is an intermediate structure e) minimum#4 is a PPII type structure.

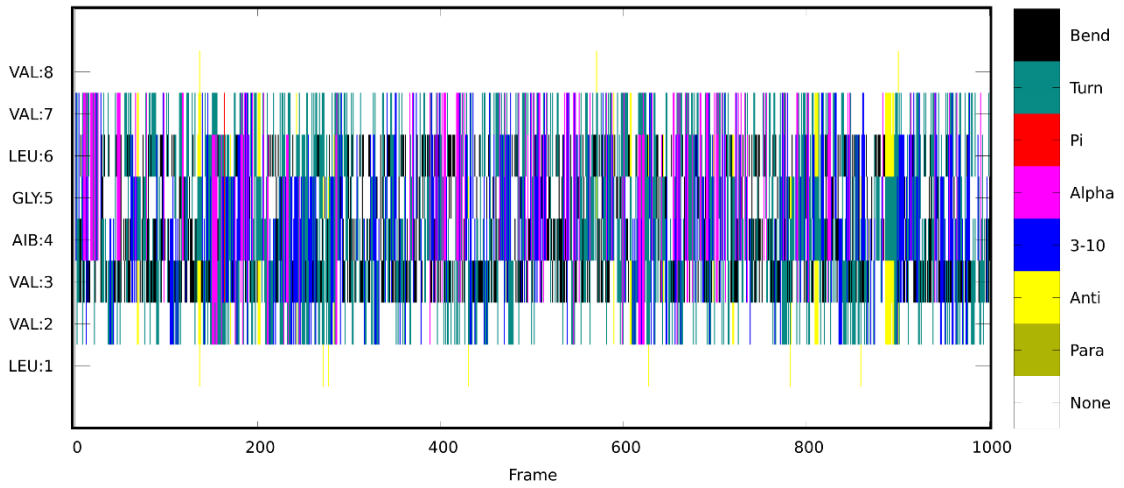


**Figure 15.** Time-dependent evolution of the secondary structure in MeOH computed taking one snapshot every 10 ns at regular intervals. Calculations were performed using the DSSP procedure [34].

Figure 15 shows the time-dependent evolution of the secondary structure per residue during the sampling process, computed using the DSSP procedure [34]. Inspection of the Figure confirms the results deduced from the cluster analysis. Despite that peptide conformational exchange is very rapid, it can be distinguished a large number of structures with a bend at Val$^3$, Aib$^4$ or Leu$^6$, together with turns at Aib$^4$ and Gly$^5$ that can be classified as Ω-shaped structures. Furthermore, helical structures as well as hairpin turns distributed in the plot are also distinguishable at diverse sections of the sampling process accounting with around 10% each, in agreement with the results from the cluster analysis.

Figures 16 and 17 depict radial distributions of methanol molecules around the peptide central residues. Specifically, distributions depicted in Figure 16 were computed using the positions of the amide hydrogen of diverse residues and the MeOH oxygen atom, including residues of the segment 2 to 7. On the other

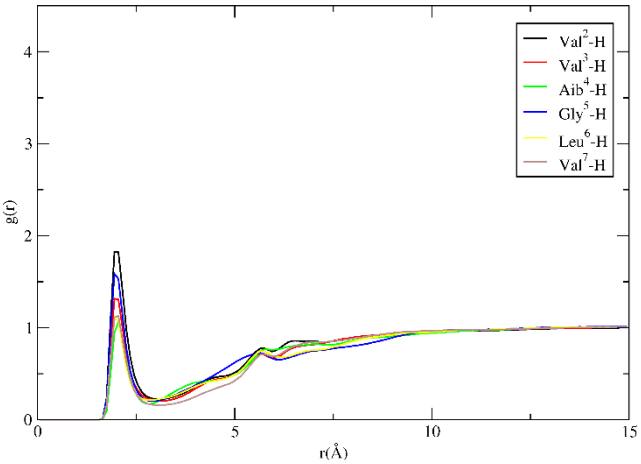


**Figure 16.** Radial distributions of MeOH molecules (O atom) around diverse backbone amide hydrogens of the peptide central segment including residues 2-7.

hand, radial distribution functions depicted in Figure 17 were computed using the amide oxygen of diverse residues and the MeOH hydroxyl hydrogen, including residues 2 to 7.

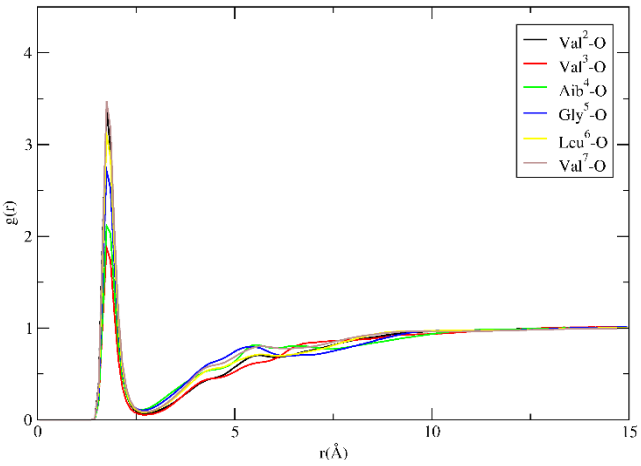


**Figure 17.** Radial distributions of MeOH molecules (hydroxyl oxygen) around diverse backbone amide oxygens of the peptide central segment including

Inspection of Figures 16 and 17 shows similar solvent distributions for the six residues, with peaks around 2 Å. However, in general hydrogen amides appear to be more exposed to the solvent than oxygen amides, since the latter exhibit smaller areas, with Aib[4], Leu[6] and Val[7] being the smallest. On the other hand, inspection of oxygen amides distributions suggest that Val[3] and Aib[4] participate in intramolecular interactions, whereas the rest are highly solvent exposed. This is consistent with Ω-shaped structures that exhibit a high exposure to the solvent. Moreover, these distributions also support the presence of helical structures, as well as β-turns in view of the lower exposure of some of the residues. Thus, the lower solvent exposure of the carbonyl oxygens of Val[3] and Aib[4], together with the lower solvent exposure of the amide hydrogen of Leu[6] and Val[7] suggests a scheme of hydrogen bonds consistent with the transient presence of helical structures. Similarly, the lower solvent exposure of the

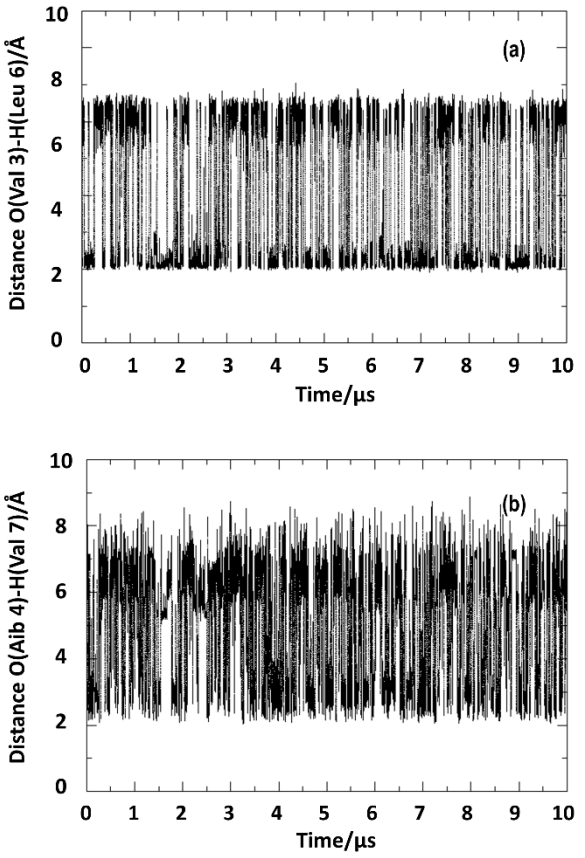


**Figure 18.** Atomic distance time evolution for the simulation in MeOH. a) between Val[3] carbonyl oxygen and Leu[6] amide hydrogen; b) between Aib[4] carbonyl oxygen and Val[7] amide hydrogen.

carbonyl of Aib[4] and the amide hydrogen of Leu[6] also supports the presence of β-turns like those shown in the structures of Figure 14b or Figure 14d.

The time-evolution of the distance between the Val[3] carbonyl oxygen and the Leu[6] hydrogen amide (Figure 18a), as well as the distance between Aib[4] carbonyl oxygen and Val[7] amide hydrogen (Figure 18b) were also analyzed. The former is consistent with a hydrogen bond ~80% of the sampling time, whereas in the latter is ~50%. When the two Figures are compared, it is clear that there are points where the two distances are consistent with a hydrogen bond that likely to correspond to helical structures. Whereas there are structures where the former is consistent with a hydrogen bond and the latter is around 6Å, structures that can be associated with a hairpin turns.

*Simulation of the peptide in water*

Likewise, as with the rest of the simulations we carried out a PCA analysis of the trajectory of the peptide in water. Figure 19 shows pictorially the projection of the 1,000,000 snapshots onto the subspace defined by the two first principal components (PC1 and PC2). In this case, the map is richer showing 5 basins in a low dimension representation of the free energy landscape. Representative structures are also shown in the Figure.

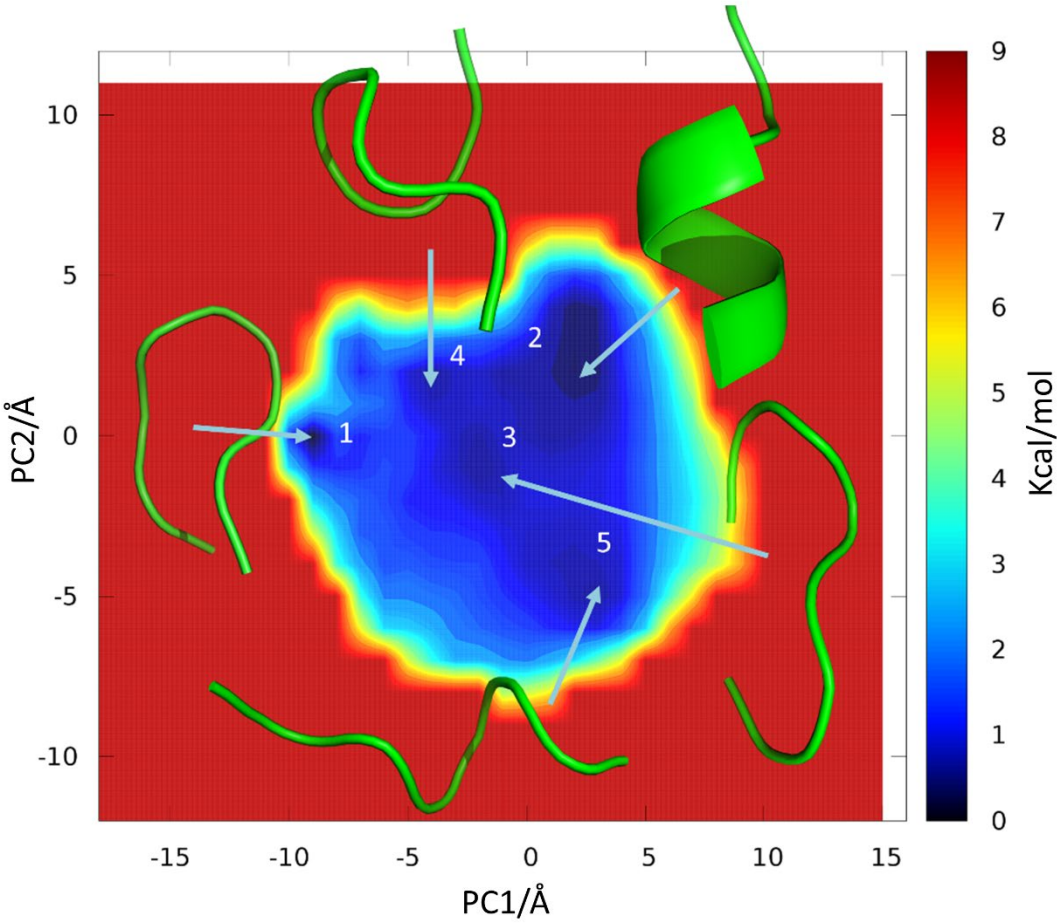


**Figure 19.** Projection of the peptide configurations sampled during the MD calculation in water onto the space defined by the two first Principal Components. Relative free energies are depicted in a color code being dark blue the lowest, in such a way that five low energy basins can be distinguished. Arrows indicate the position of the lowest energy point in each of the basins, together with the associated structure depicted in a ribbon representation.

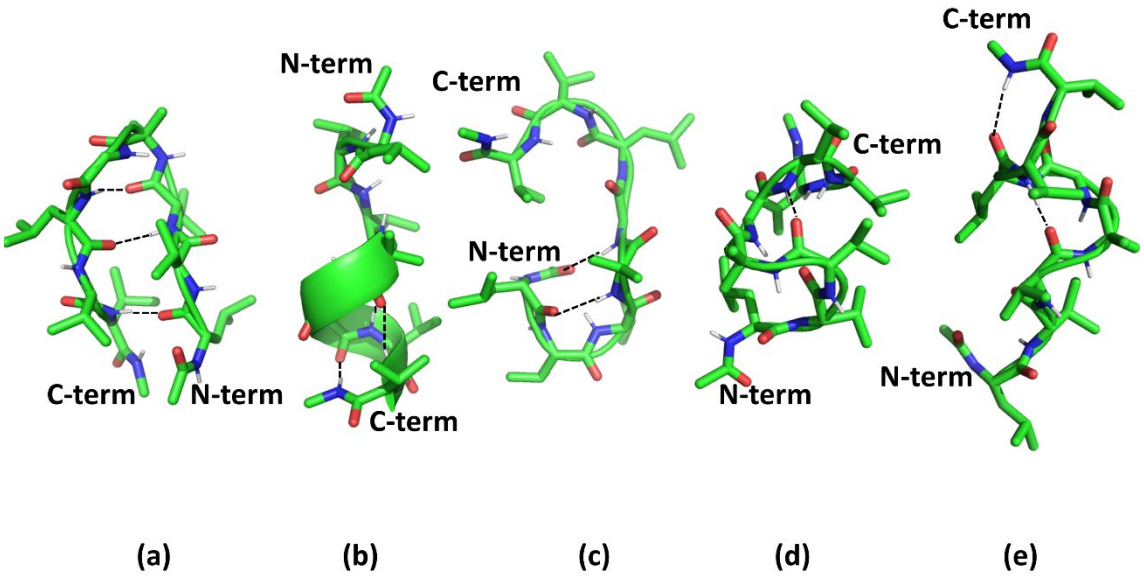


**Figure 20.** Structures of lowest energy conformations identified in the water sampling where dotted lines represent hydrogen bonds using as default geometrical features a O…H distance [2.0-3.0Å] and a NH…O angle <180°. a) minimum#1 is a hairpin structure exhibiting hydrogen bonds Leu$^{1}$(C=O)…(NH)Val$^{8}$; Val$^{3}$(NH)…(C=O)Leu$^{6}$; and Val$^{3}$(C=O)…(NH)Leu$^{6}$; b) minimum#2 is a partial helical structure exhibiting a pattern of hydrogen bonds between the carbonyl oxygen of residue i and the amide hydrogen in residue i+4; c) minimum#3 is a C-shape structure with β-turns at both termini; minimum 4 is an intermediate structure; d) minimum#5 is a Ω-shape structure with a β-turn in the central segment of the peptide and PPII or ϒ-turns at the termini.

Minimum #1 is located at coordinates (-9,0) in a basin accounting for ~22% of the population, as deduced from the cluster analysis. The structure corresponds to a distorted hairpin turn, exhibiting hydrogen bonds between the carbonyl oxygen of Leu$^{1}$ and the amide hydrogen of Val$^{8}$, the amide hydrogen of Val$^{3}$ and the carbonyl oxygen of Leu$^{6}$ and the carbonyl oxygen of Val$^{3}$ and the amide hydrogen of Leu$^{6}$, as shown pictorially in Figure 20a. Minimum #2 is located at coordinates (2,4) in a basin accounting for ~40% of the population, as deduced from the cluster analysis. Structures in this cluster correspond to helical structures at the C-terminus, exhibiting a pattern of hydrogen bonds between the carbonyl oxygen of residue i and the amide hydrogen in residue i+4, as shown in Figure 20b. Minimum #3 located at coordinates (-2,-1) is in a basin accounting for ~16% of the population, as deduced from the cluster analysis. These structures with several β-turns can be considered to exhibit a C-shape (Figure 20c). Low energy minimum #4 is located at coordinates (-4,-2) in a shallow basin representing ~8%

of the population, as deduced from the cluster analysis. Structures in this basin correspond to distorted hairpins as had been observed previously, acquiring a structure that reminds the runner of a sled, as shown pictorially in Figure 20d. Finally, low energy minimum #5 is located at coordinates (3, -5) in a shallow basin accounting for ~14% of the population, as deduced from the cluster analysis. Structures in this basin correspond to PPII conformations along several residues, as shown in Figure 20e.

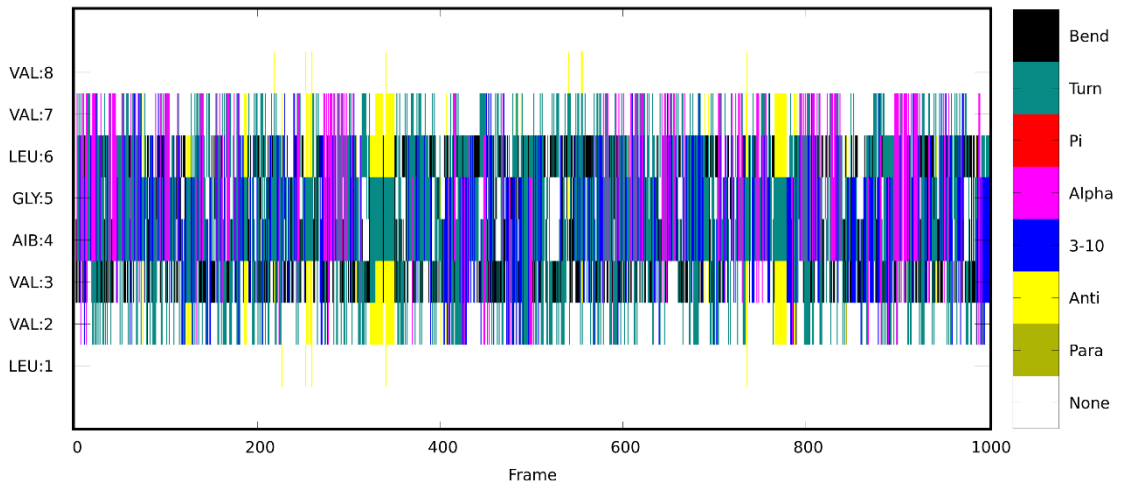


**Figure 21.** Time-dependent evolution of the secondary structure in DMSO computed taking one snapshot every 10 ns at regular intervals. Calculations were performed using the DSSP procedure [34].

Figure 21 shows the time-dependent evolution of the secondary structure per residue during the sampling process, computed using the DSSP procedure [34]. As can be seen conformational exchange in water is not as fast as in MeOH, possibly due to its higher viscosity, double than MeOH [43]. This in turn, makes the residence times of specific secondary structures longer. Inspection of the plot suggests around 20% of the structures $\alpha$-helical and almost another 20% exhibit a $3_{10}$ helix in the middle segment. Moreover, about 10% of the structures adopt a hairpin turn and the rest can be considered as Ω-shaped with turns at diverse residues or bends at $Val^3$ and $Leu^6$.

Figures 22 and 23 depict radial distribution functions of water molecules around the peptide central residues. Distributions depicted in Figure 22 were computed using the positions of the amide hydrogen of diverse residue s and the water oxygen atom, including residues 2-7. Interestingly, the area under the peaks shown in Figures 22 and 23 is smaller than the observed in Figures 16 and 17, suggesting that these residues are less exposed in water than in MeOH.

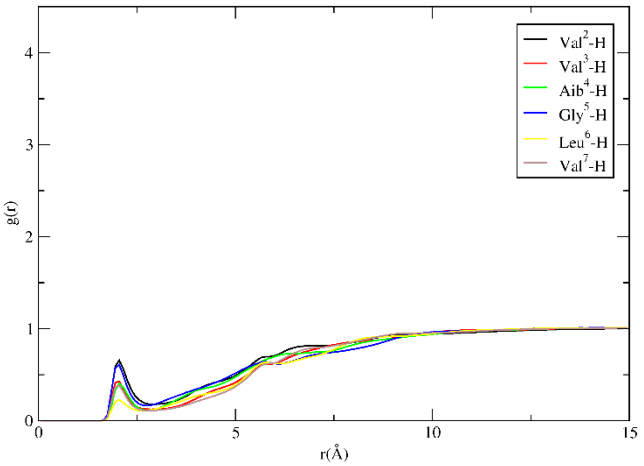


**Figure 22.** Radial distributions of water molecules (O atom) around diverse backbone amide hydrogens of the peptide central segment including residues 2-7.

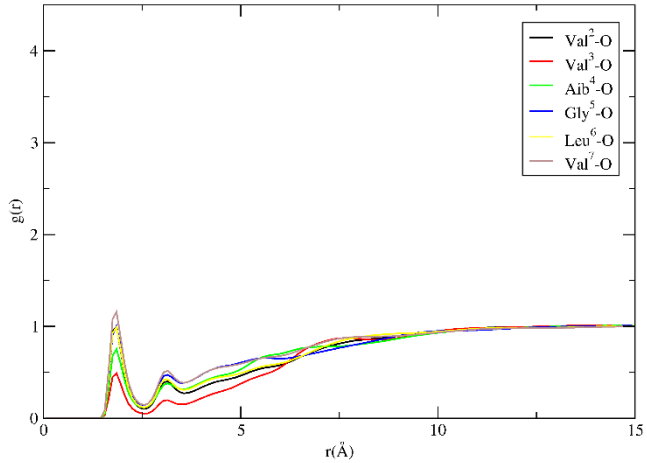


**Figure 23.** Radial distributions of water molecules (H atom) around diverse backbone amide oxygens of the peptide central segment including residues 2-7.

Inspection of Figure 22 show similar solvent distributions for the six residues, with peaks around 2 Å. Moreover, the Leu$^6$ amide hydrogen is the least exposed, followed by those of Val$^3$ and Aib$^4$. On the other hand, inspection of Figure 23 shows similar solvent distributions for the six residues, with peaks around 2 Å with a satellite around 4 Å. However, the area under the peak is not the same for all the residues. Specifically, as observed in MeOH the amide oxygen of Val$^3$ is least exposed, followed by the amide oxygen of Aib$^4$ as shown on MeOH. These distributions suggest a scheme of hydrogen bonds consistent with the peptide adopting either β-hairpin or helical conformations.

Time evolution of the distance between the Val[3] carbonyl oxygen and the Leu[6] hydrogen amide (Figure 24a) as well as the distance between the Aib[4] carbonyl oxygen and the Val[7] amide hydrogen (Figure 24b) were analyzed. In the former, the distance is consistent with a hydrogen bond ~80% of the sampling time, whereas in the latter it is ~50%. When the two Figures are compared, it is clear that there are points where the two distances are consistent with a hydrogen bond that likely to correspond to helical structures. Whereas there are structures where the former is consistent with a hydrogen bond and the latter is around 6Å, structures that can be associated with a hairpin turns.

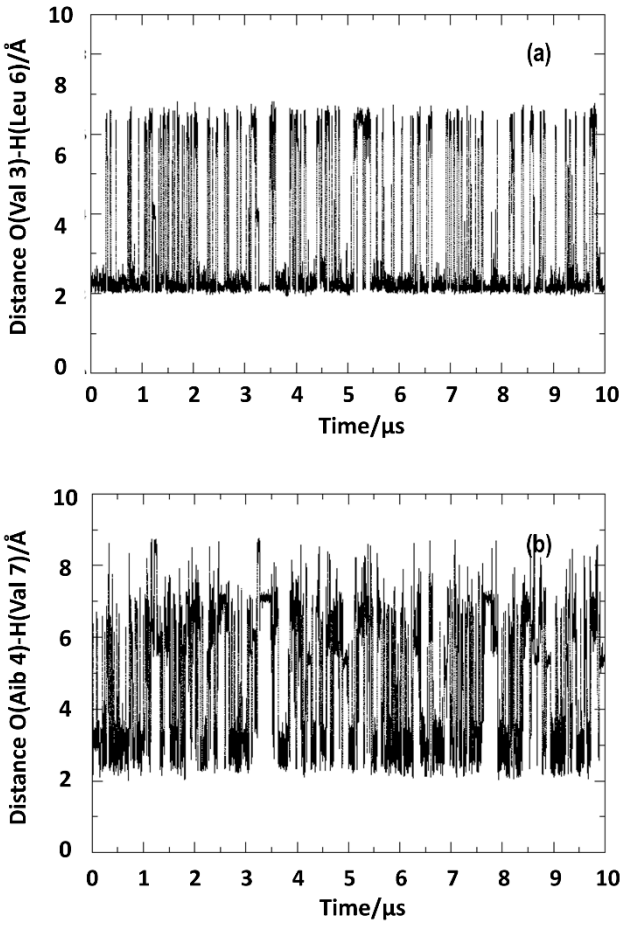


**Figure 24.** Atomic distance time evolution for the simulation in water. a) between Val[3] carbonyl oxygen and Leu[6] amide hydrogen; b) between Aib[4] carbonyl oxygen and Val[7] amide hydrogen.

## DISCUSSION

The results of the present work show dramatic differences of the conformational profile of the Balaram's peptide in diverse solvents, confirming previous results [12]. Interestingly, due to the aliphatic nature of its side chains, the differential behavior is determined by the ability of the peptide backbone atoms to establish, either intramolecular or intermolecular interactions, and this is directly connected to the capacity to form hydrogen bonds of the solvent as well as its dielectric constant to screening electrostatic interactions. In addition, the capacity of the solvents to stabilize aliphatic side chains needs also to be considered.

Present results show that the peptide quite frequently exhibits a β-turn involving residues Aib[4]-Gly[5] at the i+1 and i+2 positions in different solvents (Figures 4, 10, 15, 21). This secondary structure is sustained by a hydrogen bond between the Val[3] carbonyl oxygen and the Leu[6] amide hydrogen, as suggests inspection of the time evolution of the distance between these atoms during the sampling process (Figures 7a, 12a, 18a, 24a). This is an expected result, since the dipeptide is known to act as structural scaffold to establish type I' β-turns [12, 35]. Actually, this knowledge was used in the strategy followed for designing the Balaram's peptide, envisaging the role of the Aib[4]-Gly[5] dipeptide as nucleation site of its conformational transitions [12]. Present results also confirm that the preference for a type I' β-turn is not altered by the characteristics of the solvent, similarly as observed for the dipeptide Aib-D-Ala and in contrast to the behavior exhibited by the D-Pro-Gly dipeptide that exhibits different types of β-turns in diverse solvents [36]. Accordingly, the conformational profile of the octapeptide object of this study can be described in terms of a robust type I' β-turn conformation in the central segment Val[3]-Aib[4]-Gly[5]-Leu[6], with its termini adopting diverse conformations with higher or lower solvent exposure, depending on the characteristics of the solvent, determining exhibiting helical, hairpin turns or Ω-shape structures.

Chloroform is a nearly non-polar, aprotic solvent with low dielectric constant (ε=4.8), low dipole moment (1.15 D) and limited hydrogen bond forming capacity. So, the solvent is expected to enhance peptide intramolecular hydrogen bonds. However, it should be beard in mind that chloroform exhibits a slight capability to form hydrogen bonds with backbone carbonyl oxygens [37] and in addition, chloride atoms exhibit high electron density to produce interactions with proton donors, like backbone amide hydrogens [38].

Analysis of the simulation in chloroform clearly supports that the peptide adopts a $3_{10}$ helical conformation in this solvent. First, the free energy surface shows a large population of helical conformations (~80%) (Figure 3a), sorted in a large basin. Moreover, the time evolution of the secondary structure per residue (Figure 4) shows that after the first μs, the peptide adopts a helical structure. As can be seen, the peptide adopts mainly a $3_{10}$ helix, although in a dynamic exchange with a few $\alpha$-helix structures.

The low population of $\alpha$-helices is expected due to the low polarity of the solvent [39]. Analysis of the solvent radial distribution functions around amide hydrogens shows limited ordering of solvent molecules (Figure 5), suggesting that the peptide adopts conformations that exhibits intramolecular hydrogen bonds exclusively. Moreover, another piece of information reinforcing the adoption of a helical structure, comes from the high occupation time of two consecutive hydrogen bonds. Specifically, the time evolution of the distance between $Val^3$ carbonyl oxygen and $Leu^6$ amide hydrogen, as well that between $Aib^4$ carbonyl oxygen and $Val^7$ amide hydrogen shown in Figures 7a and 7b suggests high occupation times of hydrogen bond interactions. Finally, it should also be considered that solvent exposed non-polar side chains of the peptide are stabilized through hydrophobic interactions with chloride atoms of solvent molecules. However, despite the supporting evidence for a favored helical conformation, solvent radial distributions around carbonyl oxygens show peaks around 2.5 Å (Figure 6), suggesting intermolecular hydrogen bonds with the solvent, being more frequent with the carbonyl oxygens of residues at both termini (Figure 6). Analysis of the helical structures points out that angles N-H… O are <180º, as expected for intramolecular hydrogen bonds [40], allowing chloroform hydrogens to establish a weak interaction with the backbone carbonyl groups that give rise to the peaks observed. In summary, present results permit to conclude that the peptide adopts a helical conformation in chloroform as a result of the formation of intramolecular hydrogen bonds, favored by a weak electrostatic screening of the solvent molecules [41]. These results agree well with the conclusions derived from NMR and CD spectrometry studies [12].

DMSO is a polar, aprotic solvent with relative small dielectric constant ($\varepsilon$=46.8), and high dipole moment (4.0 D). It also exhibits a high capacity to form hydrogen bonds as acceptor, through its sulfonyl group. Actually, quantum mechanics calculations predict that hydrogen bonding between DMSO and an amide hydrogen is stronger than that between a carbonyl oxygen and an amide hydrogen [42]. Taking into consideration DMSO capacity to form hydrogen bonds and its concomitant effect of screen electrostatic interactions, it is expected to render a scenario where the peptide can establish a higher number of ligand-solvent intermolecular interactions than in chloroform.

Present results confirm that the conformational profile of the peptide in DMSO is different to the one observed in chloroform. Specifically, the peptide exhibits structures with the backbone exposed, as corroborated by the solvent distributions around residues Val[2], Val[3], Aib[4] or Gly[5] (Figure 11). Moreover, analysis of time evolution of the conformation per residue (Figure 10) shows a dominant role of the β-turn involving residues Aib[4]-Gly[5] in positions i+1 and i+2, stabilized by an intramolecular hydrogen bond between the Val[3] carbonyl oxygen and the Leu[6] amide hydrogen that is confirmed by inspection of Figure 12a. However, in contrast to the simulation with chloroform, the hydrogen bond is hold only ~70% of the sampling time. Structures displaying this hydrogen bond include the hairpin turn -the lowest energy conformation- covering a ~21% population (Figure 9a), helical structures (Figure 9b) covering ~27% and a subset of ~40% of those populating minimum#4 basin (Figure 9c), where the chain exhibits structures like γ-turns or PPII at both termini.

Comparison of the time evolution of the distance between the carbonyl oxygen and the amide hydrogen of the pair of residues Val[3]- Leu[6] (Figure 12a) and Aib[4]-Val[7] (Figure 12b), shows the dynamics of the conformational exchange. The process is relatively slow, probably due to the solvent ability to stabilize solvent exposed non-polar side chains through the formation of hydrophobic pockets by means of DMSO methyl groups [42] and its viscosity, near the double of water and four times that of MeOH [43]. Thus, inspection of Figure 10 permits to distinguish stretches where the peptide attains hairpin turns as in the interval 3-6 μs or, helical structures like in the interval 6-8 μs of the simulation.

Published results from NMR and CD spectrometry studies of the peptide in this solvent are consistent with structures like a β-turn conformation (Figure 9c) and a β-hairpin (Figure 9a) [12]. These structures represent together >40% of the population making them the preponderant population. Nevertheless, there is also a non-negligible population of ~27% of helical structures (Figure 9 d). Accordingly, present results permit to fine-tune the conclusions derived from the NMR and CD spectrometry studies that advocate for a majority of a β-hairpin conformation in this solvent. However, present results suggest the presence of a non-negligible percentage of helical conformations.

Methanol is a polar, protic solvent with a similar dielectric constant as DMSO (ε=32.6), but with a larger capacity to form hydrogen bonds through its alcohol functional group, since it can function either as a hydrogen bond donor or acceptor. Accordingly, it is expected that methanol will screen intramolecular interactions in a similar fashion as DMSO, but offering an increased hydrogen bond capability.

Analysis of the structures identified during the sampling process shows the presence of the β-turn involving the central segment $Val^3$-$Aib^4$-$Gly^5$-$Leu^6$, although in this case, the hydrogen bond between the $Val^3$ carbonyl oxygen and the $Leu^6$ amide hydrogen is hold only a 50% of the sampling process (Figure 18a). On the other hand, analysis of the free energy surface shows a similar profile that the one found in DMSO. Around 73.5% of the structures adopt a Ω-shape conformation (Figures 14b and 14d), ~13% a partial helical structure (Figure 14a) and about 9.5% of the structures exhibit β-hairpin conformation (Figure 14b). Accordingly, it can be deduced that around 96% of the structures exhibit the hydrogen bond between the $Val^3$ carbonyl oxygen and the $Leu^6$ amide hydrogen, similar to DMSO. In contrast, an interesting difference in regard the behavior shown in DMSO is the rapid conformational exchange exhibited (Figure 18a) that can be explained by its lower viscosity together with an improper solvation of the non-polar side chains.

Radial distributions of MeOH molecules exhibit low intensity peaks at around 2 Å. Inspection to the radial distribution functions around amide hydrogens (Figure 16) pinpoints that those of $Aib^4$, $Leu^6$ and $Val^7$ are the least exposed. On the other hand, radial solvent distributions around carbonyl oxygens (Figure 17) distinguish that those of $Val^3$ and $Aib^4$ are the least exposed to the solvent. The former is engaged in a hydrogen bond with the $Leu^6$ amide hydrogen in 50% of the structures (Figure 18a), whereas the latter is engaged in a hydrogen bond with the $Val^7$ amide hydrogen in 20% of the structures (Figure 18b). In addition, the lower integration area of the $Aib^4$ carbonyl is attributable to its involvement in β-turns with N-terminus residues, as can be seen in the structures shown in Figures 14b and 14d.

In conclusion, the peptide in methanol exhibits a conformational profile similar to the one found in DMSO, with about a ~86% structures attaining either a β-hairpin

(Figure 14c) or a Ω-shape with a β-turn in the central segment (Figure 14b) that make them the preponderant population. Nevertheless, there is also a non-negligible population of ~14% of helical structures (Figure 14a). Accordingly, present results permit to fine-tune the conclusion derived from the NMR and CD spectrometry studies in this solvent that advocate for a majority of a β-hairpin conformation. However, a non-negligible percentage of helical conformations should also be considered [12].

Finally, water is the most polar of the solvents studied, with a high dielectric constant (ε=78.5) and capacity to accept and donate hydrogen bonds. Accordingly, it is expected that water will screen intramolecular interactions heavily and also provides a good hydrogen bond capability. In contrast, water cannot stabilize solvent exposed non-polar side chains.

Analysis of the structures identified during the sampling process show the presence of the β-turn involving the central segment $Val^3$-$Aib^4$-$Gly^5$-$Leu^6$. In this case, the hydrogen bond between the $Val^3$ carbonyl oxygen and the $Leu^6$ amide hydrogen is beheld a 73% of the sampling process (Figure 24a). This residence time is similar to that found for DMSO, however the dynamics of the conformational exchange is much larger probably due to its smaller viscosity [44]. Looking at the solvent distribution functions, all peptide bond atoms are less exposed than in methanol, being the least exposed the amide hydrogen of $Leu^6$ and the amide oxygen of $Val^3$, reinforcing the persistence of a β-turn over the central segment of the peptide.

In water, the peptide exhibits a richer conformational profile than in other solvents so, that classification of structures is less clear-cut. The features of the solvent make that non-polar side chains tend to be buried, with valine known to be one the most helix disruptors in water [45]. Accordingly, it is expected that the peptide adopts transient partial helical conformations. A bout 19% of the structures are β-hairpin (Figure 20a) and ~20% are classified as partial helical structures (Figure 20b). This suggests that ~34% of the structures exhibit a β-turn that are not either hairpin or helix, like the structure of Figure 16e. Structures exhibiting β-turns at both termini are also populated (Figure 20c). According, the profile of the peptide in water is similar to that observed in DMSO and MeOH exhibiting a fast conformational exchange between conformations. Most of them

can be characterized by a β-turn involving residues Val[3]-Aib[4]-Gly[5]-Leu[6] with a predominance of β-hairpin and Ω-shape structures.

## CONCLUSIONS

This paper describes the results of 10 μs molecular dynamics trajectories of the Balaram's peptide in chloroform, DMSO, MeOH and water using explicit solvent simulations. Analysis of the results shows that the central β-turn formed between the Val[3] carbonyl oxygen and the Leu[6] amide hydrogen is persistent during the sampling process in all the solvents investigated. In chloroform is 100%, in DMSO 70%, in MeOH 50% and in water 73%. Moreover, the conformational profile of the peptide can be explained in terms of this central segment β-turn conformation, together with peptide termini adopting diverse conformations with higher or lower solvent exposure, depending on the characteristics of the solvent.

Present results support that in chloroform enhances intramolecular interactions increasing the adoption of helical conformations in agreement with NMR and CD studies. In the rest of the solvents, backbone atoms are more exposed and a diversity of structures are available. Thus, in DMSO with a strong capacity to form hydrogen bonds and low dielectric constant, a population of ~21% adopts a β-hairpin conformation. Comparison with NMR and CD studies suggest that the Ω-shaped conformations including a β-turn in the central segment also fulfilled the experimental results, concluding that actually the mixture of the two populations explain the observed spectra, fining-tune previous conclusions. In MeOH, the peptide exhibits a similar behavior than in DMSO, with ~12% structures either exhibiting a β-hairpin and a ~26% a Ω-shape including a β-turn in the central segment. This result permits also to fine-tune previous conclusions. However, in contrast to the profile in DMSO, in MeOH there is a rapid exchange between conformations. Finally, in water the peptide exhibits a more complex conformational profile with diversity of structures, where the hairpin turn is about half the weight of helical structures. There is also a rapid exchange between conformations, although slower than in MeOH, possibly due to its higher viscosity.

Acknowledgements

This research was funded by the Generalitat de Catalunya, grant number 2017SGR1033. We acknowledge financial support from the grant MDM-2017-0767 of the Spanish Structures and Excellence María de Maeztu program.

**REFERENCES**


1. N. Sewald and H.-D. Jakubke, *Peptides: Chemistry and Biology*. 2nd Ed. John Wiley-VCH GmbH, Weinheim, 2009.
2. L. Nevola, E. Giralt, *Chem. Commun.*, 2015, **51**, 3302—3315.
3. J. J. Perez, R. A. Perez and A. Perez, *Front. Biomol. Sci.*, 2021, **8**, 681617.
4. K. Tao, P. Makam, R. Aizen and E. Gazit, *Science*, 2017, **358**, eaam9756.
5. K. Fu, H. Wu and Z. Su, *Biotechnol. Adv.*, 2021, **49**, 107752.
6. J.J. Perez, F. Corcho and O.Llorens, *Curr. Med. Chem.*, 2002, **9**, 2209-2229.
7. J.J. Perez, *Curr. Top. Med. Chem.*, 2018, **18**, 566-590.
8. Z. Shi, C. A. Olson, G. D. Rose, R. L. Baldwin and N. R. Kallenbach, *Proc. Natl. Acad. Sci. U. S. A.,* 2002, **99**, 9190–9195.
9. M. Mezei, P. J. Fleming, R. Srinivasan and G. D. Rose, *Proteins: Struct., Funct., Genet.*, 2004, **55**, 502–507.
10. J. Graf, P. H. Nguyen, G. Stock and H. Schwalbe, *J. Am. Chem. Soc.,* 2007, **129**, 1179–1189.
11. R. Schweitzer-Stenner, *Mol. BioSyst.*, 2012, **8**, 122–133.
12. S. K. Awasthi, S.C. Shankaramma, S. Raghothama and P. Balaram, *Biopolymers*, 2001, **58**, 465-476.
13. W. Li, M. Qin, Z. Tie and W. Wang, *Phys. Rev. E.*, 2011, **84**, 041933
14. J.F. Griffin, D.A. Langs, G.D. Smith, T.L. Blundell, I.J. Tickle and S. Bedarkar *Proc. Natl. Acad. Sci. U. S. A.*, 1986, **83**, 3272-3276.
15. C. Weber, G. Wider, B. Von Freyberg, R. Traber, W. Braun, H. Widmer and K.Wuthrich, *Biochemistry*, 1991, **30**, 6563-6574.
16. P. H. Kussie, S. Gorina, V. Marechal, B. Elenbaas, J. Moreau, A.J. Levine and N.P. Pavletich, *Science*, 1996, **274**, 948-953.
17. S. Tashiro, M. Tominaga, Y. Yamaguchi, K. Kato and M. Fujita, *Angew. Chem. Int. Ed.*, 2006, **45**, 241 –244
18. N. Prabhu and K. Sharp, *Chem. Rev.,* 2006, **106**,1616-1623.
19. J. Rubio-Martinez, M.S. Tomas and J.J. Perez, *J. Mol. Graphics Model.*, 2017, **78**, 118-128.
20. W. Damm and W. F. van Gunsteren, *J. Comput. Chem.*, 2000, **21**, 774–787.
21. J.J. Perez, M.S. Tomas and J. Rubio-Martinez, *J. Chem. Inf. Model.*, 2016, **56**, 1950-1962.
22. J.J. Perez, *Biomedicines*, 2021, **9**, 651.
23. P. Cieplak, J. Caldwell and P. Kollman, *J. Comput. Chem.*, 2001, **22**, 1048–1057.
24. H. Liu, F. Müller–Plethe and W. F. van Gunsteren, *J. Am. Chem. Soc.*, 1995, **117**, 4363-4366.
25. W.L. Jorgensen, D.S., Maxwell and J. Tirado-Rives, *J. Am. Chem. Soc.*, 1996, **118**, 11225–1123.

26. W.L. Jorgensen, J. Chandrasekhar, J. Madura and M. Klein, *J. Chem. Phys.*, 1983, **79**, 926–935.
27. D. A. Case, R. M. Betz, D. S. Cerutti, T. E. Cheatham III, T. A. Darden, R. E. Duke, T. J. Giese, H. Gohlke, A. W. Goetz, N. Homeyer, S. Izadi, P. Janowski, J. Kaus, A. Kovalenko, T. S. Lee, S. LeGrand, P. Li, C. Lin, T. Luchko, R. Luo, B. Madej, D. Mermelstein, K. M. Merz, G. Monard, H. Nguyen, H. T. Nguyen, I. Omelyan, A. Onufriev, D. R. Roe, A. Roitberg, C. Sagui, C. L. Simmerling, W. M. Botello-Smith, J. Swails, R. C. Walker, J. Wang, R. M. Wolf, X. Wu, L. Xiao and P. A. Kollman, *AMBER 2016*, University of California, San Francisco, (2016).
28. J.A. Maier, C. Martinez, K. Kasavajhala, L. Wickstrom, K.E. Hauser and C. Simmerling, *J. Chem. Theory Comput*., 2015, **11**, 3696–3713
29. H. Berendsen, J. Postma, W. van Gunsteren, A. DiNola, J. Haak, *J. Chem. Phys.*, 1984, **81**, 3684–3690.
30. T. Darden, D. York and L. Pedersen, *J. Chem. Phys.*, 1993, **98**, 10089-10092.
31. J-P. Ryckaert, G. Ciccotti and H.J.C. Berendsen, *J. Comput. Phys.*, 1977, **23**, 327-341.
32. I. Daidone and A. Amadei, *WIREs Comput. Mol. Sci.*, 2012, **2**, 762-770.
33. L. Rokach and O. Maimon, *Clustering methods.* In *Data Mining and Knowledge Discovery Handbook;* O. Maimon and L. Rokach, *Eds.*, Springer: New York, NY, 2005; Chapter 15, pp. 321-352.
34. W. Kabsch and C. Sander, *Biopolymers*, 1983, **22**, 2577-2637.
35. L. R. Masterson, M. A. Etienne, F. Porcelli, G. Barany, R. P. Hammer, G. Veglia, *Biopolymers*, 2007, **88**, 746-53.
36. Y. K. Kang, H. S. Park, *New J. Chem.*, 2016, **40**, 8565-8578.
37. Jeffrey, G.A. *J. Mol. Struct.*, 1999, **485–486**, 293-298.
38. Y. Lu, Y. Liu, Z. Xu, H. Li, H. Liu and W. Zhu, *Expert Opin. Drug Discov.*, 2012, **7**, 375-383.
39. P. Pengo, L. Pasquato, S. Moro, A. Brigo, F. Fogolari, Q. B. Broxterman, B. Kaptein, P. Scrimin, *Angew. Chem. Int. Ed.*, 2003, **42**, 3388-3392.
40. D. Herschlag and M. M. Pinney, *Biochemistry*., 2018, **57**, 3338-3352.
41. P. E. Smith and J. J. Tanner, *J. Mol. Recognit.*, 2000, **13**, 27–34.
42. Y. J. Zheng and R. L. Ornstein, *J. Am. Chem. Soc.*, 1996, **118**, 4175.
43. A.M.S. Duarte, C.P.M. van Mierlo and M.A. Hemminga, *J. Phys. Chem. B*, 2008, **112**, 8664–8671
44. L.-M. Omota , O. Iulian , O. Ciocîrlan and I. Niţă. *Rev. Roum. Chim.*, 2008, **53**, 977–988
45. B. Mayer and C. Th. Klein, *J. Mol. Struct. (Theochem)*, 2000, **532**, 213-226.